# NJC

Accepted Manuscript


This is an *Accepted Manuscript*, which has been through the Royal Society of Chemistry peer review process and has been accepted for publication.

*Accepted Manuscripts* are published online shortly after acceptance, before technical editing, formatting and proof reading. Using this free service, authors can make their results available to the community, in citable form, before we publish the edited article. We will replace this *Accepted Manuscript* with the edited and formatted *Advance Article* as soon as it is available.

You can find more information about *Accepted Manuscripts* in the Information for Authors.

Please note that technical editing may introduce minor changes to the text and/or graphics, which may alter content. The journal's standard Terms & Conditions and the Ethical guidelines still apply. In no event shall the Royal Society of Chemistry be held responsible for any errors or omissions in this *Accepted Manuscript* or any consequences arising from the use of any information it contains.

ROYAL SOCIETY OF CHEMISTRY

www.rsc.org/njc

Journal Name

ARTICLE

# Synthesis of high-quality graphene sheets in task-specific Ionic liquids and their photocatalytic performance

Youyi Yu[a], Zhen Han[a], Yongbo Zhang[a], Bing Dong[a], Aiguo Kong*[a] and Yongkui Shan*[a]

A novel method for preparing high-quality graphene sheets by the liquid-phase exfoliation of expanded graphite (EG) in task-specific ionic liquids (TSILs) was developed. The used TSILs contains alkyl-3-methylimidazolium cation that has stronger intercalation in the expanded graphite and peroxydisulfate anion that oxidize the edge of the expanded graphite and facilitate the intercalation of the imidazole cation. Such coordication attack of the anion oxidation and the cation intercalation resulted in sufficient exfoliation of EG and provide single- and few-layer graphene sheets with the fewer defects, lateral extent of more than ten micrometers and higher optical transmittance. The nanocomposites comprising the prepared graphene sheets and P25 exhibit a higher photocatalytic activity for the photodegradation of methylene blue under UV-light.

## 1 Introduction

Graphene or the graphene sheets consisting of few-layer graphene have the potential to revolutionize diverse applications from smartphones and ultrafast broadband to drug delivery and computer chips.[1-5] Consequently, techniques for the scalable production of high-quality, solution-processable graphene are needed. Numerous synthesis ways including micromechanical cleavage [6] and liquid-phase [7,8] and electrochemical exfoliation[9] have been developed for the preparation of graphene sheets using the natural graphite flakes as the raw materials, provides feasible means for producing graphene with a low number of defects, although in a rather low yield. By comparison, chemical exfoliation of graphite oxide in liquid-phase is the method more widely used for the preparation of graphene in practice (Hummers' method). Unfortunately, by such chemical treatment, the original crystalline structure of the graphene basal plane is not completely restored and numerous chemical defects are introduced into the resulting graphene sheets. Expanded graphite (EG) prepared by rapid heating of the graphite intercalation compounds (GICs) has recently emerged as an important industrial raw material for the production of large-scale flexible graphite flakes. The EG keeps a layered structure similar to natural flake graphite but with large interlayer spacing, which is very beneficial for the exfoliation of EG into the graphene sheets. The graphene sheets obtained from EG have been reported.[10-12] Recently, electrochemical[13-15] and direct exfoliation of EG into the few layers graphene sheets using ionic liquids have been proposed.[16-18] The obtainment of the graphene sheets from these methods is advantageous in terms of simplicity and high volume production. However, the graphene sheets produced by these simple techniques still contain a few impurities (F and S etc.)[16] or sheet sizes of 0.006-0.0125 $\mu m^2$ are dominant representing 50% of the total distribution[18] or the graphene dispersions in ionic liquid have to be further separated for a wide range of applications.[13-18]

In this study, an improved method was presented for using EG to prepare high-quality the single-layer or few-layer graphene sheets in the oxidizing task-specific ionic liquids, 1-butyl-3-methylimidazolium peroxydisulfate ($[C_4mim]_2[S_2O_8]$), under mild conditions with high yield (~70 wt%). The procedure of preparation was described briefly in Scheme.1

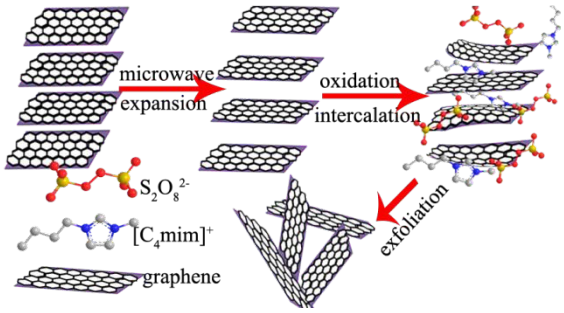


Scheme.1 Schematic diagram for preparation of graphene sheets by the oxidation and exfoliation process of EG

In recent years, the composites of graphene and semiconductor $TiO_2$[19-22] are considered as promising photocatalyst with high efficiency and low cost for air and water purification and elimination of pollutant in the environment.[23-27] The photodegradation efficiency of nanocomposite photocatalysts depends on the morphology of $TiO_2$ and the quality of graphene, which works as an electron acceptor in the composite. The band gap and defect density in the graphene component is associated with the preparation procedures. In some cases, minimizing the graphene defects can facilitate the diffusion of the photoexcited electrons to the reactive sites, which obviously enhance titania nanocomposite-based photocatalytic reduction of $CO_2$.[28] The development of more convenient and efficient technique for the

[a] School of Chemistry and Molecular Engineering, East China Normal University, 500 Dongchuan Road, Shanghai 200241, P.R. China.

fabrication of high quality graphene-based nanomaterial is crucial important for the practical applications.

The graphene sheets obtained by this method are large-sized, have only a few defects and can be used to prepare the photocatalysts with the excellent activity toward the degradation of methylene blue (MB) under UV by combination with P25 ($TiO_2$: 20% rutile and 80% anatase). The thin films formed on surface of glass slide by dip-coating method using their suspensions in water or organic solvents exhibit a higher optical transmittance.

## 2 Experimental

**2.1 Chemicals:**

Expandable graphite was purchased from Nanjing JiCang nanotechnology Co., Ltd. 1-bromobutane, acetone, ethyl acetate and potassium peroxydisulfate are obtained from Sinopharm Chemical Reagent Co., Ltd. P25 ($TiO_2$:20 % rutile and 80 % anatase) were purchased from Degussa. N-methyl imidazole was supplied by Zhejiang chemical plant and was further purification by distillation before use. The others chemicals were used as received without further treatment.

**2.2 Syntheses**

**2.2.1 $[C_4mim]_2[S_2O_8]$**

1-butyl-3-methylimidazolium bromide $[C_4mim][Br]$ was synthesized by the reaction of N-methylimidazole (0.1mol) with 1-bromobutane (0.1 mol) in a flask under refluxing at 70-75 °C for 48 h.[29] After the temperature of the reaction mixture was cooled to room temperature, the precipitated crystals was recrystallized three times from ethyl acetate, then dried in vacuum oven at 70 °C for 2 days prior to use. $[C_4mim]_2[S_2O_8]$ was prepared by the metathesis reaction between $[C_4mim][Br]$ and $K_2S_2O_8$ in acetone at room temperature,[30] in which the mole ratio of $[C_4mim][Br]$ to $K_2S_2O_8$ is 2:1. The formed KBr as a white solid was removed by filtration. The acetone was then separated from the product by rotary evaporation (<30 °C). The products were stored in a vacuum dryer before use.

**2.2.2 Graphene sheets**

Expansion of expandable graphite was carried out by the method reported in the literature.[31] The as-prepared EG (50 mg) was uniformly dispersed in 10 ml of $[C_4mim]_2[S_2O_8]$ with the help of ultrasonic cleaning instrument (sonics, 750 W, 55 KHz). This mixture was kept at 80 °C for 24 h under constant stirring, and then was dialyzed in a dialysis bag (retained molecular weight: 8000-14000 Da) overnight at room temperature to remove the ILs ($[C_4mim]_2[S_2O_8]$), subsequently dispersed in 100 ml of deionized water under ultrasonication for 60 min. The separation of the un-exfoliated expanded graphite from the mixture by centrifugation at 5000 rpm for 5 min generates dark-gray aqueous dispersions of the graphene sheets. After the water was removed from the aqueous dispersions, the prepared graphene sheets were obtained and denoted as Igraphene. For the sake of comparison, the graphene sheets were prepared from natural graphite powder (99.9 %) using modified Hummers' method[32] and denoted as Hgraphene.

**2.2.3 P25-graphene composite.**

In the typical procedure for synthesizing P25-graphene composite, 2 mg of the Igraphene was dispersed in the solution of distilled water (20 mL) and ethanol (10 mL) by ultrasonic treatment for 1 h, and then 0.2 g of P25 was added to the mixture and stirred for another 2 h to get a homogeneous suspension, which was then sealed into a Teflon-lined autoclave (40 mL), followed by hydrothermal treatment at 120 °C for 3 h. After the autoclave was cooled to room temperature, the precipitate was collected, centrifuged, washed with distilled water for three times, and dried in a vacuum oven overnight at 80 °C and recorded as P25-Igraphene. For comparison, P25-graphene composite (with the same the content of carbon, 1 wt %) were synthesized using Hgraphene as the carbon source via the method mentioned above and recorded as P25-Hgraphene.

**2.2.4 Graphene films**

For facilitating the deposition of the prepared graphene sheets on the quartz glass slide substrates easily, the 'piranha solution' (7:3 v/v $H_2SO_4/H_2O_2$) was used to rinse the substrate. Subsequently, the substrate was washed three times with DI water, followed by sonicating in DI water for 30 min. Graphene film on the substrates was prepared by dip-coating technique on dip-coating equipment (SYDC-200, DIP COATER) using the graphene sheets aqueous suspension. Transmittance of the films was measured using UV-vis spectroscopy (UV-8000 spectrophotometer) and reaches to 91% at a wavelength of 550 nm.

**2.3 Characterizations**

The morphology of the as-synthesized samples was investigated by a JEOL-2100F transmission-electron microscope (TEM) at an acceleration voltage of 200 kV and a Hitachi S-4800 field emission-scanning electron microscope (SEM). The atomic force microscope (AFM) images of the graphene samples are obtained by Vecco multimode Ⅷ on a mica plate substrate, operating in tapping mode. X-ray photoelectron spectroscopy (XPS) measurements were performed on Axis Ultra DLD using Al Kα radiation. All of the binding energies at various peaks were calibrated using the binding energy of C1s (284.5 eV). Raman spectra were taken by a Nicolet DXR Raman spectrometer from Thermo Fisher Scientific with a He-Ne lasers excitation wavelength of 633 nm at room temperature. X-ray powder diffraction (XRD) patterns were collected with a D8-Advance diffractometer (Bruker, Germany) with Cu Kα radiation, λ= 1.1514 nm. The $SO_4^{2-}$ from the reduction of peroxydisulfate can be detected by the addition of the solution containing $Ba^{2+}$ into the reaction mixture at the end of reaction.

**2.4 Photocatalytic experiments**

Investigation for the photocatalytic performance of the catalysts was completed in the quartz reactor of 50 mL with cooling water jacket. The selected photocatalyst (30 mg) was dispersed in methylene blue (MB) solution to achieve a concentration of <1 mg $mL^{-1}$. The initial dyes (MB) concentration was controlled at 10 mg $L^{-1}$. Before irradiation, the suspension was stirred for 1 h in the dark to achieve the adsorption-desorption equilibrium. Under stirring, a 100 W high pressure mercury lamp was positioned at the center of the quartz reactor as light source. In the reaction procedure, 3 mL of the reaction mixture was extracted at various irradiation times, centrifuged to remove the photocatalysts and analyzed by a UV-Vis spectrophotometer to determine the concentration of residual MB in the reaction mixture.[33] Blank experiments (without catalyst) were also carried out in order to establish the effect of photolysis and catalysis on the conversion of MB.

## 3 Results and discussion

### 3.1 Characterization of the materials

After undergoing the microwave irradiation, the expandable graphite was changed into the flake graphite or expanded graphite as shown in Fig. 1. It is clearly seen that the expanded graphite has the laminated structure with staggered voids space, which can remarkably enhance the interaction between the ionic liquid and the graphite layers.

EG was subjected to an exfoliation process in $[C_4mim][S_2O_8]$ to obtain a dark-gray aqueous dispersions. After a few weeks, Tyndall effect can still be observed when a beam of light is passed through such suspensions as shown in Fig. 2(B). It indicates that the prepared single-layer or few-layer graphene sheets were stable and without aggregation in the suspensions.[16]

TEM images in Fig. 3 clearly display that the prepared graphene sheets with a width exceeding a dozen of micrometers and some corrugations or ripples, which are very thin and stable under the electron beam. The inset in Fig. 3(B) is the corresponding SAED patterns for the graphene sheets with a typical six-fold symmetry, confirming its single crystal nature. Furthermore, HRTEM image for the edges of the sheets demonstrated that the prepared graphene sheets possess the thickness of single or few-layer graphene sheets in a large domain (Fig. 3(C) (D)).

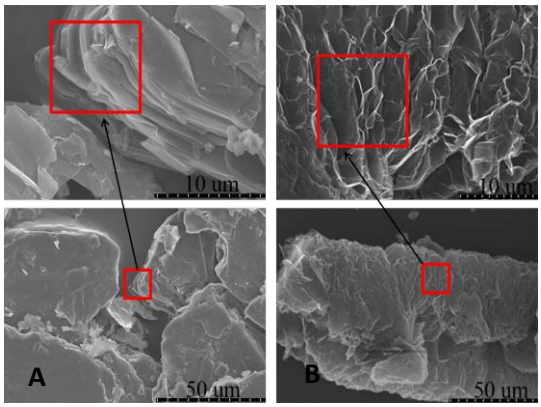


Fig.1 SEM images of expandable graphite before (A) and (B) afterheat treatment in a microwave oven (upper images: the enlarged image of (A) and (B) respectively)

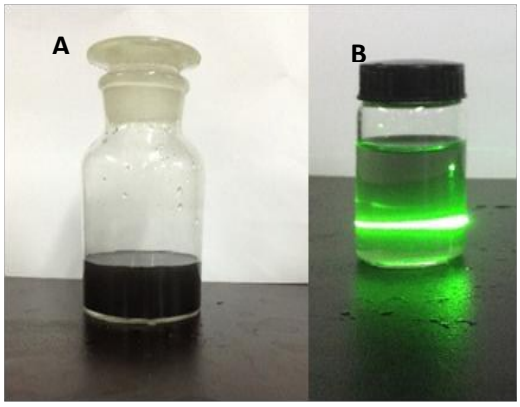


Fig.2 (A) stable graphene aqueous suspension prepared from ionic liquid exfoliation and (B) the Tyndall effect of a diluted graphene suspension

AFM analysis was performed to further characterize the morphology and thickness of the prepared graphene sheets. Fig. 4 gives the sizes of the identified graphene sheets range from 0.5 µm to 3 µm. Height profiles along the black line in (A) shown in Fig. 4(B) exhibit a plateaus with height of 0.7±0.02 nm, which is lower than the heights (~0.9 nm) of single-layer graphene prepared by exfoliating graphite using general chemical method.[34] This phenomenon corroborates that the single-layer graphene sheets with comparatively few groups containing oxygen were prepared under the mild conditions by this method. In addition, we have completed the measurement of AFM images of several graphene samples to estimate the percentage of monolayer, bilayer or few-layers. By analysis the AFM images in Fig. 5, we can estimate that the percentage of monolayer is about 45 %, the percentage of bilayer about 45 %, only a small part (about 10 %) is few-layer.

For further examining the quality of the prepared graphene sheets, Raman and XPS measurements have been conducted. The typical Raman spectra of EG and the prepared graphene sheets were shown in Fig. 6(A). The most prominent features in the Raman spectra of graphene are the G band appearing at about 1580 $cm^{-1}$ associated with the doubly degenerate (in-plane transverse (iTO) and longitudinal optical (LO)) phonon mode, G' band at

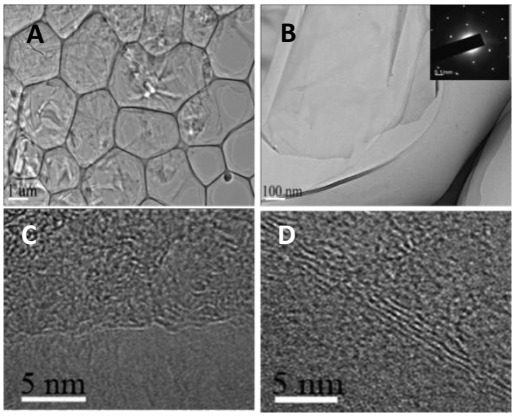


Fig.3 (A) General view of the as-synthesized graphene sheets with a width of dozens of micrometers (B) TEM view of the graphene with an inset of its corresponding selected area electron diffraction (SAED) (C-D) HRTEM of few-layer graphene sheets

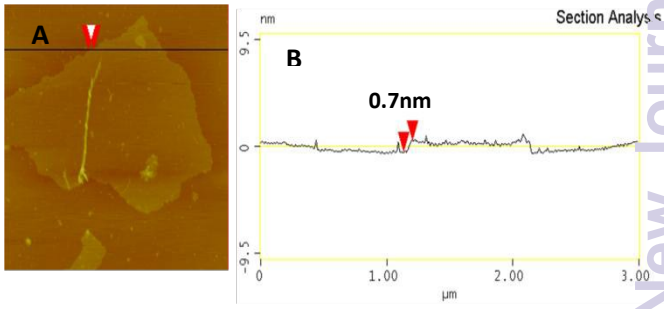


Fig.4 (A) A typical tapping mode AFM image of the prepared graphene sheets deposited on a mica substrate (B) height profile along the line shown in (A)

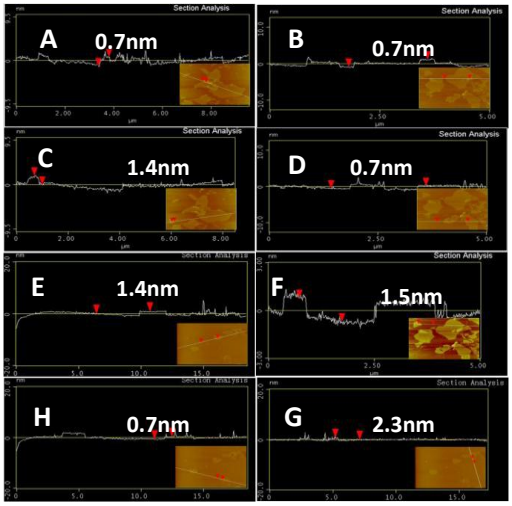


Fig.5 AFM images (A-H) of the prepared graphene sheets and their corresponding height profile along the line shown in (A-H) for estimation of the percentage of monolayer, bilayer or few-layers graphene

about 2700 $cm^{-1}$ originating from a two (iTO) phonon double resonance Raman process and D band at around 1350 $cm^{-1}$ corresponding to a second-order process involving one iTO phonon and one defect.[35] The occurrence of the D peak for EG samples and the prepared graphene sheets may be ascribed to the edge effect and the defects.[36] The intensity ration of the D to G band ($I_D/I_G$) in the Raman spectroscopy of the prepared graphene sheets is 0.29 higher than that of the EG. It suggests a slightly higher defect density of the graphene sheets was formed after undergoing the mild oxidation of EG in TSILs. However, this intensity ratio is several times smaller than that of the graphene sheets prepared by Hummers' method ($I_D/I_G$=1.22),[37] and indicates that the concentration of defects is very lower in the prepared graphene sheets. In addition, the peak deconvolution of G' band (Fig. 6(B)) prepared in $[C_4mim]_2[S_2O_8]$ shows that the prepared graphene sheets are composed of bilayer graphene.[35, 38-40]

The wide-survey XPS spectra of the graphene sheets and the EG were shown in Fig. 7(A). A strong C1s peak at 284.5 eV and a small O1s peak at 532.6 eV were observed in the spectra (Fig. 7(A)). Based on the ratio of peak area of O1s to C1s, the oxygen content of 7.6 % in the prepared graphene sheets was determined. It is slightly higher than the oxygen content of 3.4 % in the EG and substantially smaller than the oxygen content of 36.3 %[41] in few-layer graphene sheet prepared by the conventional oxidation exfoliation of graphite (Hummers' method). The C1s signal of the prepared graphene sheets consists of three different components and can be deconvoluted into three peaks at positions 284.5, 286.3 and 287.1 eV. These peaks correspond to the sp2 carbons (graphitic C=C species),[42,43] the sp3 carbons (C-OH, 5.8%)[44,45] and the oxygen-carbon groups (C–O–C, 4.5 %),[45] respectively (Fig. 7(B)). At the same time, the C 1s spectra of the EG can be deconvoluted into two peaks around 284.5 eV for the C=C in aromatic rings and 286.4 eV for the C single bonded to hydroxyl in C-OH groups (4.6 %), as seen in Fig. 7(B). These results demonstrate a small amount of carbon atoms were functionalized to form the oxygenated functional groups in the preparation procedure. This further confirms that the

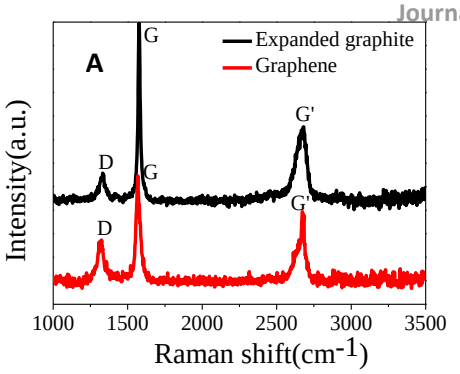


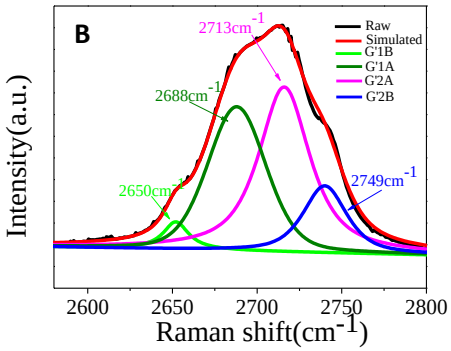


Fig. 6(A) Raman spectra of EG and the Graphene sheets (B) Fitting curves of 2D-band in the Raman spectra of the graphene sheet

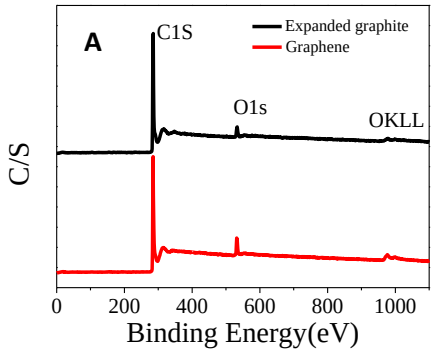


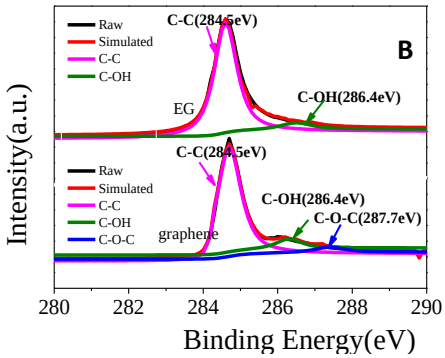


Fig. 7(A) wide-survey XPS spectra of the graphene sheets and the expanded graphite (B) C1s spectra of the EG (upper) and the Graphene sheets (down)

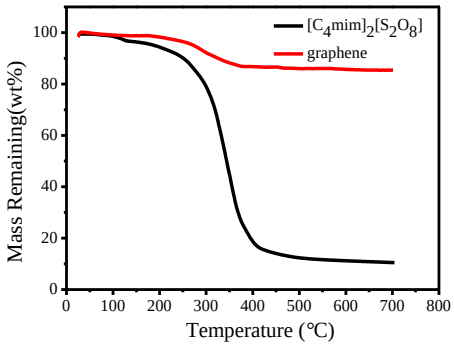


Fig. 8 TG analysis for $[C_4mim]_2[S_2O_8]$ and the obtained graphene

graphene sheets prepared in the specific task ionic liquids possess the lower density of defect.

The result of thermogravimetry analysis (TGA) of the ionic liquids and the obtained graphene sheets was shown in Fig. 8. In the TG curve of the ILs, a little weight loss (about 4 %) at 95 °C was observed, which was attributed to the decomposition of the peroxydisulfate anion.[30] In the TG curve of the prepared graphene sheets, the mass loss (~10 %) takes place around 200 °C and was ascribed to the decomposition of the oxygen functional groups present in the graphene sheets.[46-48] The result confirms the complete removal of the ILs ($[C_4mim]_2[S_2O_8]$) from the prepared graphene sheets.

The investigation results mentioned above indicated that the use of task- specific ionic liquid results in effective exfoliation of the EG to produce single or few-layer graphene sheet in high yield. This phenomenon should be ascribed to the combined action of cation and anion in the specific task ionic liquids. The cations with imidazole ring have a strong affinity to the surfaces of expanded graphite or graphene by non-covalent grafting or π-π stacking interaction and will intercalate EG at relatively low temperatures and ambient pressure.[7,14,16-19,] The peroxydisulfate anions play the role of the weaker oxidant in the reaction system, which can be further confirmed by $SO_4^{2-}$ presented in the reaction mixture at the end of reaction. The oxidized edge of the expanded graphite and facilitate the intercalation of the imidazole cation.[14] Such coordinated attack of the anion oxidation and the cation intercalation resulted in sufficient exfoliation of expanded graphite and provide the single and few-layer graphene sheets with the fewer defects in high yield.

For discovering the possibility of the prepared graphene sheets in practical utility, the thin films were prepared by dip-coating technique on the hydrophilic glass slices using the graphene sheet aqueous suspensions. The SEM image in Fig. 9(A) exhibits a continuous film with a smooth surface on the glass slices. The optical transmittance of the thin films as shown in Fig. 9(B) increases sharply with the wavelength from 80 % in the ultraviolet to 91 % in the visible region. This fact testifies that the prepared graphene sheets possess the high optical transmittance.

**3.2 Photocatalytic performance**

The graphene modified $TiO_2$ photocatalyst were widely explored because of their large specific surface areas, extraordinary electronic mobility[6], molecular stability[49] and high optical transmittance (Fig. 9) in the UV-Vis range and exhibit the high activity in most catalytic processes.[50] For purpose of identifying the

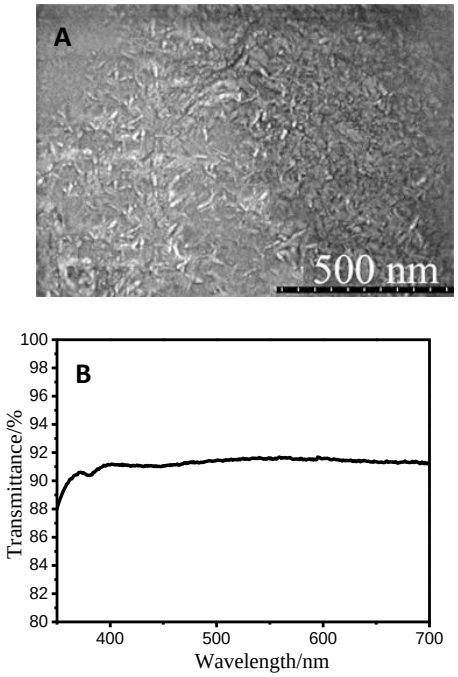


Fig.9 (A) SEM image and (B) optical transmittance curve of the prepared films

performance of the prepared graphene sheets, the P25-graphene composites photocatalysts (P25-graphene) were fabricated. Typical TEM and SEM images of P25-Igraphene in (Fig. 10 (A) (B)) indicate the P25 well dispersed on the graphene sheets, which plays a supporting role in the P25-Igraphene nanocomposite. The XRD patterns of the P25-Igraphene and pure P25 in (Fig. 10 (C)) illustrate that the crystal phase of P25 was not destroyed in the formation of P25-Igraphene.

The photocatalytic performance of the prepared P25-graphene sheet composite was evaluated by photodegradation of methylene blue under UV-light. The evolutions of MB photodegradation using different photocatalysts are shown in Fig. 10 (D). The experimental results obtained under UV irradiation for 55 minutes were displayed in Tab. 1. It is seen from Fig. 10(D) and Tab. 1 that P25-Igraphene exhibits excellent photocatalytic activity. The degradation percentage of MB over P25-Igraphene achieves 97 %, which is 14 % higher than that over P25-Hgraphene and 85 % higher than P25. The enhanced photocatalytic activity results from combining properties of graphene as paper-shape material and the unique function of P25 particles for photocatalysis. In general, under UV illumination, the electron-hole pairs can be formed when electrons in the valence band (VB) of $TiO_2$ are excited to the conduction band (CB) and are responsible for the photocatalytic activity of $TiO_2$. Unfortunately, photogenerated electron-hole pairs will very rapidly recombine before the chemical interaction of $TiO_2$ with adsorbed pollutant and it limits the photocatalytic efficiency of $TiO_2$. Graphene or graphene sheet have a 2D single atomic layer feature of graphite and has an extensive two dimensional π-π conjugation net. When combining $TiO_2$ with graphene, the graphene sheet plays a role of an electron acceptor in the composite.[51] The photoexcited electrons at the $TiO_2$-graphene or graphene sheet heterointerface can flow from $TiO_2$ to graphene or graphene sheet. Such heterointerface can efficiently separate the photoexcited

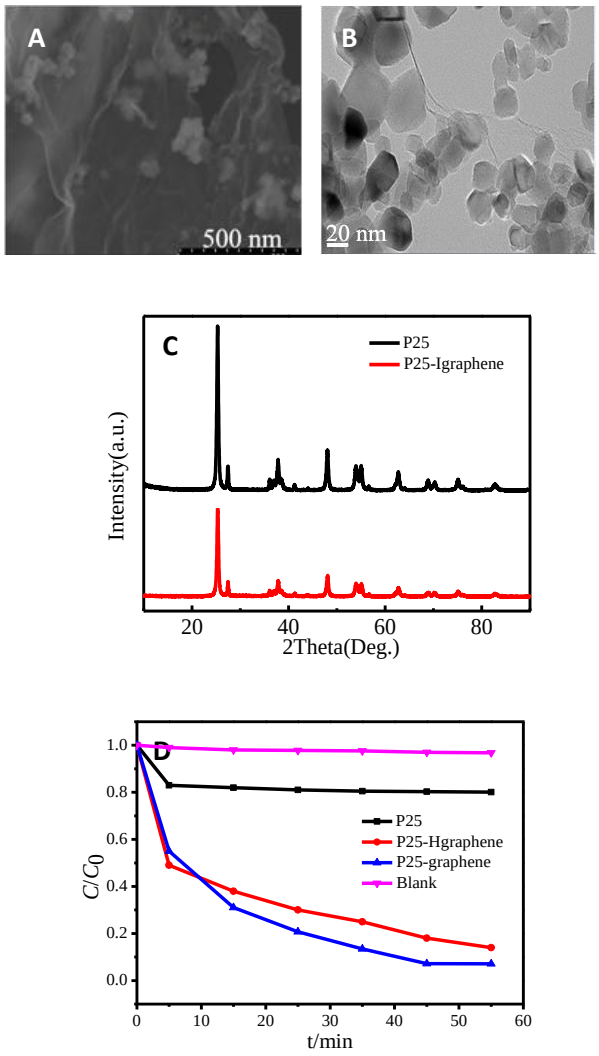


Fig. 10(A) SEM and (B) TEM image of P25-Igraphene (C) XRD pattern of P25 and P25-Igraphene (D) Photodegradation of MB under UV irradiation over different catalysts

Table 1 Results of photodegration of MB under UV over various catalysts

| Catalyst | Photodegradation efficiency (%) |
|---|---|
| Blank | 3% |
| P25 | 12% |
| P25-Hgraphene | 83% |
| P25-Igraphene | 97% |

electron-hole pairs, impede they recombination and significantly improve the photocatalytic ability. In this case, the electronic state at the heterointerface in the composite is very important for its stability and photocatalytic function and relies on the energy band structure of its component. The CB position of anatase and rutile is about -4.21 eV and -4.01 eV with a band gap of about 3.2 eV and 3.0eV, respectively (using vacuum level as a reference)[52], the calculated work function of intrinsic graphene is 4.42 eV.[53] The deficiency in graphene can convert graphene into a semiconductor, of which the band gap can be tuned by changing the defect densities of the grapheme.[54,55] In the prepared P25-graphene sheet composite, anatase-rutile junction in P25 (80 % anatase, 20 % rutile) and anatase-graphene sheet, rutile-graphene sheet and anatase-rutile-graphene sheet heterointerface may be formed by hydrothermal treatment. Electrons tend to flow from the higher to lower Fermi level through these heterointerface in the composite. Graphene sheets prepared by us have lower defect density and narrow band gap[28] and possess the lower Fermi level and the improved electrical mobility. Under UV irradiation, the photoexcited electrons can easily been transferred into the graphene sheets after the photoactivation of titanium dioxide in the prepared P25-Igraphene, photoinduced holes migrate into titania phase and the formed heterointerfaces strongly reduce recombination of electrons and hole, which result in that the less defective graphene sheet prepared by us exhibit larger photocatalytic enhancement factors compared to graphene sheet prepared by Hummers' method, especially for photo-degradation of methylene blue.

## 4 Conclusion

In this work, the new method for the preparation of the single or few-layer graphene sheet from expanded graphite in high yield was reported by utilizing the anion oxidation and the cation intercalation of the task-specific ionic liquid under the mild conditions, which endows this preparation method with efficient and eco-friendly functions. The prepared graphene sheets possess the lower density of defect and their suspensions in aqueous solution are stable and without sedimentation for several weeks. The optical transmittance of the thin films comprising the prepared graphene sheets reaches 91 %, which suggests that the prepared graphene sheets have great potential in optoelectronic applications. The investigation resulted from photo-degradation of methylene blue testify that the less defective graphene sheet prepared by us exhibit larger photocatalytic enhancement factor compared to graphene sheet prepared by Hummers' method.

## Acknowledgments

The authors are grateful for financial support from the National Natural Science Foundation (No. 21303058), the Shanghai Municipal Natural Science Foundation (No. 13ZR1412400) and the key project of Shanghai Science and Technology Committee (No. 11JC1403400;14231200300).

## Notes and references

1. F. Schwierz, *Nat. Nanotechnol*., **2010**, **5**, 487-496.
2. P. Avouris, Z. H. Chen and V. Perebeinos, *Nat. Nanotechnol*., **2007**, **2**, 605-615.
3. M. Burghard, H. Klauk and K. Kern, *Adv. Mater*., **2009**, **21**, 2586-2600.
4. H. Shinohara and A. Tiwari, John Wiley & Sons, *Graphene An introduction to the fundamentals and industrial application.* Wiley Scrivener punblishing, 2015.
5. V. F. Bonaccorso, K. S. Novoselov, S. Roche, P. Bøggild, S. Borini and F. Koppens, *Nanoscale.*, **2015**, **7**, 4598-4810.

6. K. S. Novoselov, A. K. Geim, S. V. Morozov, D. Jiang, Y. Zhang, S. V. Dubonos, I. V. Grigorieva and A. A. Firsov, *Science*., **2004**, **306**, 666-669.
7. Y. Hernandez, V. Nicolosi, M. Lotya, F. M. Blighe, Z. Y. Sun, S. De, I. T. McGovern, B. Holland, M. Byrne, Y. K. Gun'Ko, J. J. Boland, P. Niraj, G. Duesberg, S. Krishnamurthy, R. Goodhue, J. Hutchison, V. Scardaci, A. C. Ferrari and J. N. Coleman, *Nat. Nanotechnol*., **2008**, **3**, 563-568.
8. W. F. Zhao, M. Fang, F. R. Wu, F. Wu, L. W. Wang and G. H. Chen, *J. Mater. Chem*., **2010**, **28**, 5817-5819.
9. N. Liu, F. Luo, H. X. Wu, Y. H. Liu, C. Zhang and J. Chen, *Adv. Funct. Mater*., **2008**, **18**,1518-1525.
10. P. K. Ang, S. Wang, Q. L. Bao, J. T. L. Thong and K. P. Loh, *ACS. Nano*., **2009**, **3**, 3587-3594.
11. J. H. Lee, D. W. Shin, V. G. Makotchenko, A. S. Nazarov, V. E. Fedorov, Y. H. Kim, J. Y. Choi, J. M. Kim and J. B. Yoo, *Adv. Mater*., **2009**, **21**, 4383-4387.
12. X. L. Li, G. Y. Zhang, X. D. Bai, X. M. Sun, X. R. Wang, E. G. Wang and H. J. Dai, *Nat. Nanotechnol*., **2008**, **3**, 538-542.
13. A. T. Najafabadi and E. Gyenge, *Carbon*., **2014**, **71**, 58-69.
14. J. Lu, J. X. Yang, J. Z. Wang, A. lim, S. Wang and K. P. Loh, *ACS.Nano*., **2009**,**3**, 2367-2375.
15. M. Mao, M. Wang, J. Hu, G. Lei, S. Chen, and H. Liu, *Chem. Commun*., **2013**, **49**, 5301-5303.
16. X. Q. Wang, P. F. Fulio, G. A. Baker, G. M. Veith, R. R. Unocic, S. M. Mahurin, M. F. Chi and S. Dai, *Chem. Commun*., **2010**, **46**, 4487-4489.
17. D. Nuvoli, L. Valentini, V. Alzari, S. Scognamillo, S. B. Bon, M. Piccinini, J. Illescas and A. Mariani, *J. Mater. Chem*., **2011**, **21**, 3428-3431.
18. N. G. Shang, M. Li, N. G. Shang, P. Papakonstantinou, S. Sharma, G. Lubarsky, M. X. Li, D. W. McNeill, A. J. Quinn, W. Z. Zhou and R. Blackley, *Chem. Commun*., **2012**, **48**, 1877-1879.
19. A. K. Kothari, E. Konca, B. W. Sheldon, K. Q. Jian, H. Li, Z. H. Xia, W. Y. Ni and R. Hurt, *J. Mater. Sci*., **2009**, **44**, 6020-6027.
20. B. Z. Jang and A. Zhamu, *J. Mater. Sci*., **2008**, **43**, 5092-5101.
21. H. Zhang, X. J. Lv, Y. M. Li, Y. Wang and J. H. Li, *ACS. Nano*., **2009**, **4**, 380-386.
22. X. Y. Zhang, H. P. Li, X. L. Cui and Y. H. Li, *J. Mater. Chem*., **2010**, **20**, 2801-2806.
23. A. A. Balandin, S. Ghosh, W. Z. Bao, I. Calizo, D. T. F. Miao and C.N. Laul, *Nano. Lett*., **2008**, **8**, 902-907.
24. K. I. Bolotin, K. J. Sikes, Z. Jiang, M. Klima, G. Fudenberg, J. Hone, P. Kim and H. L. Stormer, *Solid. State. Commun*., **2008**, **146**, 351-355.
25. P. Steurer, R. Wissert, R. Thomann and R. Mülhaupt, *Macromol. Rapid. Commun*., **2009**, **30**, 316-327.
26. X. Huang, L. Y. Wang, J. Z. Zhou and N. Y. Gao, *Water. Res*., **2014**, **57**, 1-7.
27. J. Li, S. l. Zhou, G. B. Hong and C. T. Chang, *Chem. Eng. J*., **2013**, **219**, 486-491.
28. Y. T. Liang, B. K. Vijayan, K. A. Gray and M. C. Hersam, *Nano. Lett*., **2011**, **11**, 2865-2870.
29. S. K. Ghosh, S. K. Saha, M. C. Ghosh, R. N. Bose, J. W. Reed and E. S. Gould, *Inorg. Chem*., **1992**, **31**, 3358-3362.
30. S.Y. Shi, A.G. Kong, X. H. Zhao, Q. Y. Zhang and Y. K. Shan, *Eur. J. Inorg. Chem*., **2010**, **15**, 2283-2289.
31. L. Zhu, X. Zhao, Y. Li, X. Yu, C. Li and Q. Zhang, *Mater. Chem. Phys*., **2013**, **3**, 984-990.
32. Y. Xu, H. Bai, G. Lu, C. Li and G. Shi, *J. Am. Chem. Soc*., **2008**, **130**, 5856-5857.
33. J. Wang, H. Zhu, C. Hurren, J. Zhao, E. Pakdel, Z. Li and X. Wang, *J. Environ. Chem. Engin*., **2015**, **3**, 1437-1443.
34. X. Yang, X. Zhang, Z. Liu, Y. Ma, Y. Huang and Y. Chen, *J. Phys. Chem. C*., **2008**, **112**, 17554-17558.
35. L. M. Malard, M. A. Pimenta, G. Dresselhaus and M. S. Dresselhaus, *Phy. Rep*., **2009**, **5**, 51-87.
36. S. Stankovich, R.D. Piner, X. Chen, N. Wu, S. T. Nguyen and R. S. Ruoff, *J. Mate*r. *Chem*., **2006**, **16**, 155-158.
37. A. A. Green and M. C. Hersam, *J. Phys. Chem. Let*., **2009**, **1**, 544-549.
38. M. S. Dresselhaus, A. Jorio, M. Hofmann, G. Dresselhaus and R. Saito, *Nano. Lett*., **2010**,**10**, 751-758.
39. Z. Ni, Y. Wang, T. Yu, and Z. Shen, *Nano. Res*., **2008**, **1**, 273-291.
40. C. Cong, T. Yu, K. Sato, J. Shang, R. Saito, G. F. Dresselhaus and M. S. Dresselhaus, *ACS. Nano*., **2011**, **5**, 8760-8768.
41. H. Zhang, J. Wang, Q. Yan, W. Zheng, C. Chen and Z. Yu, *J. Mater. Chem*., **2011**, **21**, 5392-5397.
42. K. H. Park, D. Lee, J. Kim, J. Song, Y. M. Lee, H. T. Kima and J. K. Park, *Nano. Lett*., **2014**, **14**, 4306-4313.
43. K. H. Park, B. H. Kim, S. H. Song, J. Kwon, B. S. Kong, K. Kang, and S. Jeon, *Nano. Lett*., **2012**, **12**, 2871-2876.
44. N. I. Kovtyukhova, Y. Wang, A. Berkdemir, R. Cruz-Silva, M. Terrones, V. H. Crespi and T. E. Mallouk, *Nat. Chem*., **2014**, **6**, 957-963.
45. L. Zhang, Z. Zhang, C. He, L. Dai, J. Liu and L. Wang, *ACS. Nano*., **2014**, **8**, 6663-6670.
46. S. Stankovich, D. A. Dikin, G. H. B. Dommett, K. M. Kohlhaas, E. J. Zimney, E. A. Stach, R. D. Piner, S. T. Nguyen and R. S. Ruoff, *Nature*., **2006**, **442**, 282-286.
47. H. A. Becerril, J. Mao, Z. Liu, R. M. Stoltenberg, Z. Bao and Chen, Y. *ACS. Nano*., **2008**, **2**, 463-470.
48. S. Stankovich, D. A. Dikin, R. D. Piner, K. A. Kohlhaas, A. Kleinhammes, Y. Jia, Y. Wu, S. T. Nguyen and R. S. Ruoff, *Carbon.,* **2007**, **45**, 1558-1565.
49. C. Lee, X. Wei, J. W. Kysar and J. Hone, *Science*., **2008**, **321**, 385-388.
50. K. Zhou, Y. Zhu, X. Yang, X. Jiang and C. Li, *New. J. Chem*., **2011**, **35**, 353-359.
51. Q. Liu, Z. Liu, X. Zhang, L. Yang, N. Zhang, G. Pan, S. Yin, Y. Chen and J. Wei, *Adv. Funct. Mater*., **2009**, **19**, 894-904.
52. Y. Xu and M. A. A. Schoonen, *Am. Mineral*., **2000**, **85**, 543-556.
53. R. Czerw, B. Foley, D. Tekleab, A. Rubio, P. M. Ajayan and D. L. Carroll, *Phys. Rev. B. Condens. Matter*., **2002**, **66**, 033408-033412.
54. X. Wu, M. Sprinkle, X. Li, F. Ming, C. Berger and W. A. deHeer, *Phys. Rev. Lett*., **2008**, **101**, 026801-026805.
55. H. K. Jeong, M. H. Jin, K. P. So, S. C. Lim and Y. H. Lee, *J. Phys. D: Appl. Phys*., **2009**, **42**, 065418-065424.

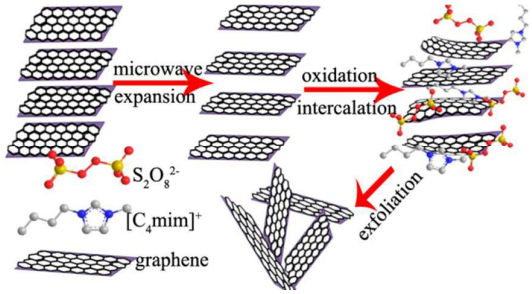


Oxidation of peroxydisulfate anion and intercalation of imidazole cation facilitates sufficient exfoliation of expanded graphite in the ionic liquids.